Supplementary Information for

Chaos in Dirac electron optics: Emergence of a relativistic quantum chimera

Hong-Ya Xu, Guang-Lei Wang, Liang Huang, and Ying-Cheng Lai

Corresponding author: Y.-C. Lai (Ying-Cheng.Lai@asu.edu)

CONTENTS

I. BASICS

The starting point of our analysis is the effective low-energy Hamiltonian of graphene or graphene-like systems with Dirac cones:

$$H = v_F s_0 \otimes \boldsymbol{\sigma} \cdot \boldsymbol{p} + s_0 \otimes \sigma_0 \mathcal{V}_{gate}(\boldsymbol{r}) - s_z \otimes \sigma_0 \mathcal{M}(\boldsymbol{r}), \tag{S1.1}$$

where the identity matrix s_0 and the Pauli matrix s_z act on the real electron spin space while the Pauli matrices $\boldsymbol{\sigma} = (\sigma_x, \sigma_y)$ and the identity matrix σ_0 define the sublattice pseudospin. The first term in Eq. (S1.1) characterizes the pristine Dirac cone band dispersion with a four-fold degeneracy at a Dirac point: two for the sublattice pseudospin and two for the real electron spin. Since $[s_z \otimes \sigma_0, H] = 0$, it is equivalent to two copies of Dirac-like Hamiltonian indexed by the spin quantum number $s = \pm$:

$$H_s = H_0 + \mathcal{V}_{gate}(\boldsymbol{r}) - s\mathcal{M}(\boldsymbol{r}), \tag{S1.2}$$

where $H_0 = v_F \boldsymbol{\sigma} \cdot \boldsymbol{p}$ is effectively the fundamental Dirac-Weyl Hamiltonian describing the two-dimensional free-space massless Dirac fermions. The Hamiltonian H_s acts on two-component pseudospinor waves for the massless Dirac quasiparticles belonging to the real spin state s in graphene or similar materials. The last two terms in Eq. (S1.1) represent the applied gate and exchange potential, respectively.

In the main text, the calculations are for the scattering of such quasiparticles from the step potential that can lead to spin-resolved ray-path defined classical dynamics in the short wavelength limit. The scattering process is of the relativistic type for massless Dirac fermions. In the following Secs. II-V, we develop an S-matrix based scheme to solve the relativistic quantum scattering problem, which is validated computationally in Sec. VI. In Sec. VII, we provide a detailed demonstration of the phenomenon of enhanced spin polarization as shown in Fig. 2(c) in the main text.

II. MULTICHANNEL ELASTIC SCATTERING THEORY FOR TWO-DIMENSIONAL MASSLESS DIRAC FERMIONS - *S*-MATRIX APPROACH

The main theoretical tool that we employ to investigate the role of chaos in Dirac electron optics is the formalism of stationary quantum scattering for two-dimensional massless Dirac fermions, where the scatterer has an irregular shape and a finite range. The scattering process is assumed to be elastic. The fundamental quantity of interest is the scattering (S-) matrix, from which all physically relevant quantities characterizing the scattering process can be deduced.

In the free space, the system is governed by the stationary Dirac-Weyl equation

$$H_0 \chi = \hbar v_F \boldsymbol{\sigma} \cdot \boldsymbol{k} \chi = E \chi, \tag{S2.3}$$

for which the plane-wave solutions for energy $E = \alpha \hbar v_F k$ is given by

$$\chi_k(\boldsymbol{r}) = \frac{1}{\sqrt{2}} \begin{pmatrix} 1 \\ \alpha e^{i\theta_{\boldsymbol{k}}} \end{pmatrix} e^{i\boldsymbol{k}\cdot\boldsymbol{r}}, \tag{S2.4}$$

where $k = \sqrt{k_x^2 + k_y^2}$, $\alpha = \mathrm{sgn}(E)$ and $\theta_{\boldsymbol{k}} = \arctan(k_y/k_x)$ characterize the propagating direction parallel to the wavevector $\boldsymbol{k}$ for $E > 0$. For $E < 0$, the two directions are anti-parallel with each other. In the polar coordinates $\boldsymbol{r} = r(\cos\theta, \sin\theta)$, the corresponding spinor cylindrical waves with given angular momentum and energy are

$${}^{k}h_m(r,\theta) = \begin{pmatrix} \mathcal{Z}_m(kr) \\ i\alpha \mathcal{Z}_{m+1}(kr) e^{i\theta} \end{pmatrix} e^{im\theta}, \tag{S2.5}$$

where $\mathcal{Z}_m$ is the m-th order Bessel or Hankel function of the physically relevant kind. In particular, under the time convention $e^{-iE/\hbar t}$ and for positive energy $E > 0$, we have

$${}^{k}h_m^{(-)} = \begin{pmatrix} H_m^{(2)}(kr) \\ iH_{m+1}^{(2)}(kr) e^{i\theta} \end{pmatrix} e^{im\theta}, \tag{S2.6a}$$

as the cylindrical wave basis of the spinor waves of the incoming type, and

$${}^{k}h_m^{(+)} = \begin{pmatrix} H_m^{(1)}(kr) \\ iH_{m+1}^{(1)}(kr) e^{i\theta} \end{pmatrix} e^{im\theta}, \tag{S2.6b}$$

as the outgoing type, where $H_m^{(1)}$ and $H_m^{(2)}$ denote the Hankel functions of the first and second kind, respectively.

For the scattering problem illustrated in Fig. 1 in the main text, the stationary wavefunction outside the scatterer generally can be decomposed into two parts - incoming and outgoing waves:

$$\Psi = \Psi_{in} + \Psi_{out}. \tag{S2.7}$$

In the spinor cylindrical wave basis for massless Dirac fermions with positive energy, the incoming wave can be written as

$$\Psi_{in} = \sum_m a_m \, {}^k h_m^{(-)}, \tag{S2.8}$$

and the outgoing wave can be expressed as

$$\Psi_{out} = \sum_m a_m \sum_{m'} S_{mm'} \, {}^k h_{m'}^{(+)}, \tag{S2.9}$$

where the coefficients a_m are determined to yield a desired kind of incoming test wave, $S_{mm'}$ denotes the transition amplitude for an incoming cylindrical wave ${}^k h_m^{(-)}$ scattered into an outgoing one ${}^k h_{m'}^{(+)}$. This defines the S-matrix with m and m' covering all possible angular momentum channels. We thus have

$$\begin{aligned}
\Psi(r,\theta) &= \sum_m a_m \left[\begin{pmatrix} H_m^{(2)}(kr) \\ iH_{m+1}^{(2)}(kr)e^{i\theta} \end{pmatrix} e^{im\theta} + \sum_{m'} S_{mm'} \begin{pmatrix} H_{m'}^{(1)}(kr) \\ iH_{m'+1}^{(1)}(kr)e^{i\theta} \end{pmatrix} e^{im'\theta} \right], \\
&= \sum_m 2a_m \begin{pmatrix} J_m(kr) \\ iJ_{m+1}(kr)e^{i\theta} \end{pmatrix} e^{im\theta} + \sum_m a_m \sum_{m'} (S_{mm'} - \delta_{mm'}) \begin{pmatrix} H_{m'}^{(1)}(kr) \\ iH_{m'+1}^{(1)}(kr)e^{i\theta} \end{pmatrix} e^{im'\theta}.
\end{aligned} \tag{S2.10}$$

To be concrete, we assume the incident wave to be a plane wave given by

$$\chi_{\boldsymbol{k}_{in}}(r,\theta) = \frac{1}{\sqrt{2}} \begin{pmatrix} 1 \\ e^{i\theta_{\boldsymbol{k}_{in}}} \end{pmatrix} e^{i\boldsymbol{k}_{in}\cdot\boldsymbol{r}} = \frac{1}{\sqrt{2}} \begin{pmatrix} 1 \\ e^{i\theta'} \end{pmatrix} e^{ikr\cos(\theta-\theta')},$$

for massless Dirac fermions with positive energy $E = \hbar v_F k$ and incident wavevector $\boldsymbol{k}_{in} = k(\cos\theta', \sin\theta')$ that makes an angle θ' with the x axis. This defines the incident propagating direction as shown in Fig. 1 in the main text. We have

$$\chi_{\boldsymbol{k}_{in}} = \sum_m \frac{i^m e^{-im\theta'}}{\sqrt{2}} \begin{pmatrix} J_m(kr) \\ iJ_{m+1}(kr)e^{i\theta} \end{pmatrix} e^{im\theta}, \tag{S2.11}$$

where the Jacobi-Anger expansion $e^{iz\cos\theta} = \sum_m i^m J_m(z) e^{im\theta}$ has been used. Given the coefficients

$$a_m = a_m(\theta') = \frac{i^m e^{-im\theta'}}{2\sqrt{2}}, \tag{S2.12}$$

and with the definition $T_{mm'} \equiv S_{mm'} - \delta_{mm'}$, we get

$$\Psi(r,\theta) = \chi_{\boldsymbol{k}_{in}} + \sum_m a_m \sum_{m'} T_{mm'} \begin{pmatrix} H_{m'}^{(1)}(kr) \\ iH_{m'+1}^{(1)}(kr)e^{i\theta} \end{pmatrix} e^{im'\theta}. \tag{S2.13}$$

Far away from the scatterer center, i.e. $kr \gg 1$, the asymptotic wavefunction can be written as

$$\lim_{kr\gg 1} \Psi = \chi_{\boldsymbol{k}_{in}} + \frac{f(\theta,\theta')}{\sqrt{-ir}} \begin{pmatrix} 1 \\ e^{i\theta} \end{pmatrix} e^{ikr}, \tag{S2.14}$$

where f is the scattering amplitude for two-dimensional massless Dirac fermions, which is related to the differential cross section through

$$\frac{d\sigma}{d\theta} \equiv \sigma(\theta,\theta') = |f(\theta,\theta')|^2, \tag{S2.15a}$$

the total cross section through

$$\sigma_t(\theta') = \oint d\theta |f(\theta,\theta')|^2, \tag{S2.15b}$$

the transport cross section through

$$\sigma_{tr}(\theta') = \oint d\theta (1-\cos\theta) |f(\theta,\theta')|^2, \tag{S2.15c}$$

and the skew cross section through

$$\sigma_{sk}(\theta') = \oint d\theta \sin\theta |f(\theta,\theta')|^2. \tag{S2.15d}$$

It follows from Eqs. (S2.13) and (S2.14) that

$$\frac{f(\theta,\theta')}{\sqrt{-ir}} \begin{pmatrix} 1 \\ e^{i\theta} \end{pmatrix} e^{ikr} = \lim_{kr\gg 1} \sum_m a_m \sum_{m'} T_{mm'} \begin{pmatrix} H^{(1)}_{m'}(kr) \\ iH^{(1)}_{m'+1}(kr) e^{i\theta} \end{pmatrix} e^{im'\theta}.$$

Finally, we obtain

$$f(\theta,\theta') = i\sqrt{\frac{2}{\pi k}} \sum_{m'} \sum_m a_m(\theta') T_{mm'} (-i)^{m'} e^{im'\theta}. \tag{S2.16}$$

Defining

$$f_l(\theta') = \sum_m a_m(\theta') T_{ml} (-i)^l = \sum_m a_m(\theta') (S_{ml} - \delta_{ml}) (-i)^l, \tag{S2.17}$$

we rewrite the scattering amplitude as

$$f(\theta,\theta') = i\sqrt{\frac{2}{\pi k}} \sum_l f_l(\theta') e^{il\theta},$$

which, when substituted into Eqs. (S2.15a)-(S2.15d), leads to convenient summation forms of the various cross sections in terms of $f_l(\theta')$ (and eventually the scattering matrix elements S_{ml}) as

$$\sigma(\theta,\theta') = \frac{2}{\pi k} \left| \sum_l f_l(\theta') e^{il\theta} \right|^2 = \frac{2}{\pi k} \sum_{l,l'} \sum_{m,m'} a_m a^*_{m'} (S_{ml} - \delta_{ml}) (S^*_{m'l'} - \delta_{m'l'}) (-i)^{(l-l')} e^{i(l-l')\theta}, \tag{S2.18a}$$

$$\sigma_t(\theta') = \frac{4}{k} \sum_l \left| f_l(\theta') \right|^2 = \frac{4}{k} \sum_{m,m'} a_m (TT^\dagger)_{mm'} a^*_{m'}, \tag{S2.18b}$$

$$\sigma_{tr}(\theta') = \sigma_t(\theta') - \frac{4}{k}\sum_l \Re[f_l f_{l+1}^*] = \sigma_t(\theta') - \frac{4}{k}\sum_{m,m'} \Re\left[ia_m\left(T\mathring{T}^\dagger\right)_{mm'}a_{m'}^*\right], \tag{S2.18c}$$

and

$$\sigma_{sk}(\theta') = \frac{4}{k}\sum_l \Im[f_l f_{l+1}^*] = \frac{4}{k}\sum_{m,m'} \Im\left[ia_m\left(T\mathring{T}^\dagger\right)_{mm'}a_{m'}^*\right], \tag{S2.18d}$$

where $(\mathring{T}^\dagger)_{lm'} \equiv (T^\dagger)_{l+1,m'} = T^*_{m',l+1}$. All the scattering cross sections are functions of θ' that defines the direction of the incident wave with respect to the x axis. Averaging over all the incident directions (θ'), we obtain the cross sections that are independent of the angle θ' as

$$\overline{\sigma}_t = \frac{1}{2\pi}\oint d\theta'\sigma_t(\theta') = \frac{4}{k}\sum_{m,m'}\frac{1}{2\pi}\oint d\theta' a_m(\theta')(TT^\dagger)_{mm'}a^*_{m'}(\theta') = \frac{1}{2k}\sum_{m,l}\left|T_{ml}\right|^2, \tag{S2.19a}$$

$$\overline{\sigma}_{tr} = \overline{\sigma}_t - \frac{4}{k}\sum_{m,m'}\Re\left[\frac{i}{2\pi}\oint d\theta' a_m(\theta')(T\mathring{T}^\dagger)_{mm'}a^*_{m'}(\theta')\right] = \frac{1}{2k}\sum_{m,l}\left\{|T_{ml}|^2 - \Re\left[iT_{ml}T^*_{m,l+1}\right]\right\}, \tag{S2.19b}$$

and

$$\overline{\sigma}_{sk} = \frac{1}{2k}\sum_l\sum_{m,m'}\Im\left[iT_{ml}(\mathring{T}^\dagger)_{lm'}\delta_{mm'}\right] = \frac{1}{2k}\sum_{m,l}\Im\left[iT_{ml}T^*_{m,l+1}\right]. \tag{S2.19c}$$

From the definition

$$T_{ml} = S_{ml} - \delta_{ml},\ \text{(i.e. } T = S - I),$$

we can calculate the characteristic cross sections once the scattering (S)-matrix is obtained.

In addition to the cross sections, associated with the S-matrix, another quantity of interest is the Wigner-Smith delay time [1, 2] defined as

$$\tau(E) = -i\hbar\mathrm{Tr}\left[S^\dagger\frac{\partial S}{\partial E}\right], \tag{S2.20}$$

which characterizes the temporal aspects of the scattering process. The delay time is related to the density of states [3] through $\rho(E) = \tau(E)/(2\pi\hbar)$.

By definition, the transport cross section most appropriately characterizes the transport property, which determines the transport relaxation time τ_{tr} according to the Fermi's golden rule with its reciprocal given by

$$\frac{1}{\tau_{tr}} = n_c v_F \sigma_{tr}, \tag{S2.21}$$

where n_c is the concentration of identical scatterers that are assumed to be sufficiently dilute so that multiple scattering effects can be neglected. If the system dimension is larger than the mean-free path $\mathcal{L} = v_F\tau_{tr}$, from the semiclassical Boltzmann transport theory, we obtain the conductivity of the system as

$$\frac{G}{G_0} = k_F v_F \tau_{tr} = \frac{k}{n_c\sigma_{tr}}, \tag{S2.22}$$

where $G_0 = 2e^2/h$ is the conductance quantum.

III. *S*-MATRIX FOR *ECCENTRIC* ANNULAR SHAPED (RING) SCATTERER

We perform an explicit calculation of the S-matrix for the scatterer of annular shape defined by two disks of different radii ($R_1, R_2 < R_1$) with a finite relative displacement ξ of the disk centers, as shown in Fig. 1(a) in the main text. For convenience, we adopt the convention that the unprimed coordinates are defined by choosing the origin as the center of the larger disk O while the primed ones have their origin at the small disk center O'. Applying the standard S-matrix formalism, we obtain the wavefunction outside the eccentric annular scatterer, i.e., $|\boldsymbol{r}| > R_1$, in the unprimed polar coordinates $\boldsymbol{r} = (r, \theta)$ as

$$\Psi^I(\boldsymbol{r}) = \sum_{m=-\infty}^{\infty} a_m^0 \left[{}^{k_0}h_m^{(2)} + \sum_{m'=-\infty}^{\infty} S_{mm'} \, {}^{k_0}h_{m'}^{(1)} \right], \tag{S3.23}$$

where $S_{mm'}$ denotes the S-matrix elements in terms of the two given channels indexed by m and m', respectively, and the coefficients a_m^0 are chosen to yield a desired kind of incident test wave. Let ${}^{k_0}\underline{h}_m^{(2)} \equiv a_m^0 \, {}^{k_0}h_m^{(2)}$ and $\underline{S}_{mm'} \equiv a_m^0 S_{mm'}$, and so

$$\Psi^I(\boldsymbol{r}) = \sum_{m=-\infty}^{\infty} \left[{}^{k_0}\underline{h}_m^{(2)} + \sum_{m'=-\infty}^{\infty} \underline{S}_{mm'} \, {}^{k_0}h_{m'}^{(1)} \right]. \tag{S3.24}$$

The wavefunction in the annular region ($|\boldsymbol{r}'| > R_2$ and $|\boldsymbol{r}| < R_1$) can be expressed in the unprimed coordinates as

$$\Psi^{II}(\boldsymbol{r}) = \sum_{m=-\infty}^{\infty} \sum_{l=-\infty}^{\infty} {}^{m}a_l^1 \left[{}^{k_1}h_l^{(2)} + \sum_{l'=-\infty}^{\infty} S_{ll'}^{od} \, {}^{k_1}h_{l'}^{(1)} \right], \tag{S3.25}$$

where the resulting matrix $S^{od} \equiv [S_{ll'}^{od}]$ characterizes the scattering from the off-centered small inner disk and is non-diagonal. Making use of the addition property of the Bessel functions, we obtain the following relation

$$S^{od} = U^{-1} S^{cd} U, \tag{S3.26}$$

where the transformation matrices $U = [U_{l\mu}] = [J_{\mu-l}(k_1\xi)]$ and $U^{-1} = [U_{ml}^{-1}] = [J_{m-l}(k_1\xi)]$ are responsible for the eccentric displacement/deformation, and $S^{cd} = [S_l^{cd}\delta_{ll'}]$ is the diagonal scattering matrix for the centered inner disk scatterer in the primed coordinates with its elements S_l^{cd} given by

$$S_l^{cd} = -\frac{\alpha_1 H_{l+1}^{(2)}(k_1R_2)J_l(k_2R_2) - \alpha_2 H_l^{(2)}(k_1R_2)J_{l+1}(k_2R_2)}{\alpha_1 H_{l+1}^{(1)}(k_1R_2)J_l(k_2R_2) - \alpha_2 H_l^{(1)}(k_1R_2)J_{l+1}(k_2R_2)}. \tag{S3.27}$$

The S-matrix of the whole scatterer can thus be determined by the matching conditions at the outer boundary $|\boldsymbol{r}| = R_1$. In Eqs. (S3.23) and (S3.25), ${}^{k_{0,1}}h_m^{(1,2)}$ denote the basic spinor waves consisting of the expanding basis indexed by the angular momentum in the polar coordinates and are explicitly given in Eq. (S5.44a). In particular, for a given incident spinor wave with angular momentum m, wavefunction matching for each momentum value j yields

$$a_m^0 H_m^{(2)}(k_0R_1)\delta_{mj} + a_m^0 S_{mj} H_j^{(1)}(k_0R_1) = {}^{m}a_j^1 H_j^{(2)}(k_1R_1) + \sum_l {}^{m}a_l^1 S_{lj}^{od} H_j^{(1)}(k_1R_1), \tag{S3.28a}$$

$$i\alpha_0\left[a_m^0 H_{m+1}^{(2)}(k_0R_1)\delta_{mj}+a_m^0 S_{mj}H_{j+1}^{(1)}(k_0R_1)\right]=i\alpha_1\left[{}^m a_j^1 H_{j+1}^{(2)}(k_1R_1)+\sum_l {}^m a_l^1 S_{lj}^{od}H_{j+1}^{(1)}(k_1R_1)\right]. \tag{S3.28b}$$

Defining matrices

$$\mathbb{X}^{(1,2)}=[H_m^{(1,2)}(k_0R_1)\delta_{mj}],\ \mathbb{Y}^{(1,2)}=[H_{m+1}^{(1,2)}(k_0R_1)\delta_{mj}], \tag{S3.29a}$$

and

$$\mathbf{x}^{(1,2)}=[H_m^{(1,2)}(k_1R_1)\delta_{mj}],\ \mathbf{y}^{(1,2)}=[H_{m+1}^{(1,2)}(k_1R_1)\delta_{mj}], \tag{S3.29b}$$

we can rewrite the above equations in the following compact form

$$\mathbb{A}^0\mathbb{X}^{(2)}+\mathbb{A}^0S\mathbb{X}^{(1)}=\mathbb{A}\mathbf{x}^{(2)}+\mathbb{A}S^{od}\mathbf{x}^{(1)}, \tag{S3.30a}$$

$$\alpha_0\left[\mathbb{A}^0\mathbb{Y}^{(2)}+\mathbb{A}^0S\mathbb{Y}^{(1)}\right]=\alpha_1\left[\mathbb{A}\mathbf{y}^{(2)}+\mathbb{A}S^{od}\mathbf{y}^{(1)}\right], \tag{S3.30b}$$

with the coefficient matrices $\mathbb{A}^0=[a_m^0\delta_{mj}]$ and $\mathbb{A}=[\,{}^m a_j^1]$. Solving the above equations, we arrive at

$$S=-\frac{\mathbb{Y}^{(2)}-\alpha_0\alpha_1\mathbb{X}^{(2)}\mathbb{T}}{\mathbb{Y}^{(1)}-\alpha_0\alpha_1\mathbb{X}^{(1)}\mathbb{T}}, \tag{S3.31}$$

where $\mathbb{T}=\mathbb{F}^{-1}\mathbb{G}$ with the conventions $\mathbb{F}=\mathbf{x}^{(2)}+S^{od}\mathbf{x}^{(1)}, \mathbb{G}=\mathbf{y}^{(2)}+S^{od}\mathbf{y}^{(1)}$ and band indices $\alpha_{0,1}=\pm 1$. Substituting the S-matrix given in Eq. (S3.31) into Eq. (S3.30a), we obtain matrix $\mathbb{A}$ consisting of the expansion coefficients ${}^m a_l^1$ in the annular region as

$$\mathbb{A}=\frac{\mathbb{A}^0\mathbb{X}^{(2)}+\mathbb{A}^0S\mathbb{X}^{(1)}}{\mathbf{x}^{(2)}+S^{od}\mathbf{x}^{(1)}}. \tag{S3.32}$$

IV. CALCULATION OF WAVEFUNCTIONS

Inside the inner disk region, i.e., $|\boldsymbol{r}'|<R_2$, the wavefunction in the primed polar coordinates $\boldsymbol{r'}=(r',\theta')$ (with origin at the small disk center O') is

$$\widetilde{\Psi}^{III}(r',\theta')=\sum_m\sum_l {}^m\widetilde{b}_l\begin{pmatrix}J_l(k_2r')\\ is_2J_{l+1}(k_2r')e^{i\theta'}\end{pmatrix}e^{il\theta'}. \tag{S4.33}$$

The expansion coefficients ${}^m\widetilde{b}_l$ can be determined by the matching condition at the inner boundary $r'=|\boldsymbol{r}-\boldsymbol{\xi}|=R_2$ between $\Psi^{(2)}(r',\theta')$ and $\Psi^{(1)}(r,\theta)$. To do so, it is convenient to reformulate the wavefunction inside the annular region in the primed coordinates. Using the relations

$$S_{ll'}^{od}=\sum_j J_{l-j}S_{jj}^{cd}J_{l'-j}, \tag{S4.34a}$$

$$\delta_{ll'}=\sum_j J_{l-j}J_{l'-j}, \tag{S4.34b}$$

and assuming $l' = j+n$, we have

$$
\begin{aligned}
{}^{k_1}h_l^{(2)} + \sum_{l'=-\infty}^{\infty} S_{ll'}^{od}\ {}^{k_1}h_{l'}^{(1)} &\equiv \sum_{l'=-\infty}^{\infty} \left[\delta_{ll'}\ {}^{k_1}h_{l'}^{(2)} + \sum_j J_{l-j} S_{jj}^{cd} J_{l'-j}\ {}^{k_1}h_{l'}^{(1)} \right], \\
&= \sum_{l'} \sum_j J_{l-j} \left[J_{l'-j}\ {}^{k_1}h_{l'}^{(2)} + S_{jj}^{cd} J_{l'-j}\ {}^{k_1}h_{l'}^{(1)} \right], \\
&= \sum_j J_{l-j} \left[\sum_n J_n\ {}^{k_1}h_{j+n}^{(2)} + S_{jj}^{cd} \sum_n J_n\ {}^{k_1}h_{j+n}^{(1)} \right].
\end{aligned} \tag{S4.35}
$$

Making use of the Graf's addition theorem [4] for the Bessel functions $Z_j \in \left\{ J_j, H_j^{(1,2)} \right\}$:

$$
Z_j(kr')e^{ij\theta'} = \sum_n J_n(k\xi) Z_{j+n}(kr) e^{i(j+n)\theta},
$$

we can rewrite the Eq. (S4.35) in the primed coordinates as

$$
{}^{k_1}h_l^{(2)} + \sum_{l'=-\infty}^{\infty} S_{ll'}^{od}\ {}^{k_1}h_{l'}^{(1)} = \sum_j J_{l-j} \left[{}^{k_1}\widetilde{h}_j^{(2)} + S_{jj}^{cd}\ {}^{k_1}\widetilde{h}_j^{(1)} \right], \tag{S4.36}
$$

where

$$
{}^{k_1}\widetilde{h}_j^{(1,2)} = \begin{pmatrix} H_j^{(1,2)}(k_1 r') \\ i\alpha_1 H_{j+1}^{(1,2)}(k_1 r') e^{i\theta'} \end{pmatrix} e^{ij\theta'}. \tag{S4.37}
$$

Substituting this expression into Eq. (S3.25), we obtain the wavefunction for the annular region in the primed coordinates as

$$
\widetilde{\Psi}^{II}(r',\theta') = \sum_m \sum_l \sum_j {}^m a_l^1 J_{l-j} \left[{}^{k_1}\widetilde{h}_j^{(2)} + S_{jj}^{cd}\ {}^{k_1}\widetilde{h}_j^{(1)} \right] = \sum_m \sum_l {}^m\widetilde{a}_l^1 \left[{}^{k_1}\widetilde{h}_l^{(2)} + S_{ll}^{cd}\ {}^{k_1}\widetilde{h}_l^{(1)} \right], \tag{S4.38}
$$

where

$$
{}^m\widetilde{a}_l^1 = \sum_j {}^m a_j^1 J_{j-l}(k_1\xi). \tag{S4.39}
$$

Imposing the continuity of the wavefunction at $r' = R_2$, we get

$$
{}^m\widetilde{b}_l = {}^m\widetilde{a}_l^1 \frac{H_l^{(2)}(k_1R_2) + S_{ll}^{cd} H_l^{(1)}(k_1R_2)}{J_l(k_2R_2)}. \tag{S4.40}
$$

With the expansion coefficients ${}^m a_l^1$, ${}^m\widetilde{a}_l^1$, and ${}^m\widetilde{b}_l$ so determined and the scattering matrices S, S^{od}, S^{cd} obtained in the relevant regions via Eqs. (S3.32, S4.39, S4.40) and Eqs. (S3.31, S3.26, S3.27), respectively, we can calculate the wavefunctions accordingly, which together give the full wavefunction in the entire space.

V. IDEAL CENTRIC CASE: ANALYTIC RESULTS

For the centric case, i.e., $\xi = 0$, we can obtain the analytic solutions of the scattering problem via the standard technique of partial wave decomposition. In particular, due to the circular rotational

symmetry and hence conservation of the total angular momentum, the partial waves outside the annular scatterer ($r > R_2$) can be written as

$$\psi_m^I = {}^{k_0}h_m^{(2)} + S_m\, {}^{k_0}h_m^{(1)}. \tag{S5.41}$$

Inside the annular region $R_1 < r < R_2$, the waves are

$$\psi_m^{II} = A_m \left[{}^{k_1}h_m^{(2)} + S_m^{cd}\, {}^{k_1}h_m^{(1)} \right] \tag{S5.42}$$

and

$$\psi_m^{III} = B_m\, {}^{k_2}\chi_m, \tag{S5.43}$$

in the inner disk region $r < R_2$, where $[k_0, k_1, k_2] = [|E_0|, |E_0 - V_1|, |E_0 - V_2|]/\hbar v$,

$${}^{k_{0,1}}h_m^{(1,2)} = \begin{pmatrix} H_m^{(1,2)}(k_{0,1}r) \\ i\alpha_{0,1}H_{m+1}^{(1,2)}(k_{0,1}r)e^{i\theta} \end{pmatrix} e^{im\theta}, \tag{S5.44a}$$

and

$$\chi_m = \begin{pmatrix} J_m(k_2 r) \\ i\alpha_2 J_{m+1}(k_2 r)e^{i\theta} \end{pmatrix} e^{im\theta}, \tag{S5.44b}$$

with $\alpha_{0,1,2} = \pm 1$ being the band index defined as the signs of $E_0, (E_0 - V_{1,2})$, respectively, and $m = 0, \pm 1, \pm 2, \cdots$ denote the orbital angular momentum. The scattering amplitudes S_m, S_m^{cd} and the expansion coefficients A_m, B_m can be determined from the boundary conditions $\psi_m^I(R_1, \theta) = \psi_m^{II}(R_1, \theta); \psi_m^{II}(R_2, \theta) = \psi_m^{III}(R_2, \theta)$, leading to the following linear matrix equation

$$\begin{pmatrix} H_m^{(2)}(k_1R_2) & -J_m(k_2R_2) & H_m^{(1)}(k_1R_2) & 0 \\ \alpha_1 H_{m+1}^{(2)}(k_1R_2) & -\alpha_2 J_{m+1}(k_2R_2) & \alpha_1 H_{m+1}^{(1)}(k_1R_2) & 0 \\ H_m^{(2)}(k_1R_1) & 0 & H_m^{(1)}(k_1R_1) & -H_m^{(1)}(k_0R_1) \\ \alpha_1 H_{m+1}^{(2)}(k_1R_1) & 0 & \alpha_1 H_{m+1}^{(1)}(k_1R_1) & -\alpha_0 H_{m+1}^{(1)}(k_0R_1) \end{pmatrix} \begin{pmatrix} A_m \\ B_m \\ C_m \\ S_m \end{pmatrix} = \begin{pmatrix} 0 \\ 0 \\ H_m^{(2)}(k_0R_1) \\ \alpha_0 H_{m+1}^{(2)}(k_0R_1) \end{pmatrix}, \tag{S5.45}$$

where $C_m \equiv A_m S_m^{cd}$. From the standard quantum scattering theory, we have that S_m is an element of the S-matrix for the concentric circular scatterer, which is diagonal in the basis of angular momentum states m. Solving Eq. (S5.45), we obtain the coefficients as

$$A_m = \frac{H_m^{(2)}(k_0R_1) + H_m^{(1)}(k_0R_1)S_m}{H_m^{(2)}(k_1R_1) + H_m^{(1)}(k_1R_1)S_m^{cd}}; \;\; B_m = A_m \frac{H_m^{(2)}(k_1R_2) + H_m^{(1)}(k_1R_2)S_m^{cd}}{J_m(k_2R_2)}, \tag{S5.46a}$$

while the scattering amplitudes for the whole scatterer are given by

$$S_m = -\frac{\alpha_0 x_m H_{m+1}^{(2)}(k_0R_1) - \alpha_1 y_m H_m^{(2)}(k_0R_1)}{\alpha_0 x_m H_{m+1}^{(1)}(k_0R_1) - \alpha_1 y_m H_m^{(1)}(k_0R_1)}, \tag{S5.46b}$$

where $x_m = H_m^{(2)}(k_1R_1) + H_m^{(1)}(k_1R_1)S_m^{cd}$ and $y_m = H_{m+1}^{(2)}(k_1R_1) + H_{m+1}^{(1)}(k_1R_1)S_m^{cd}$ with S_m^{cd} given by Eq. (S3.27).

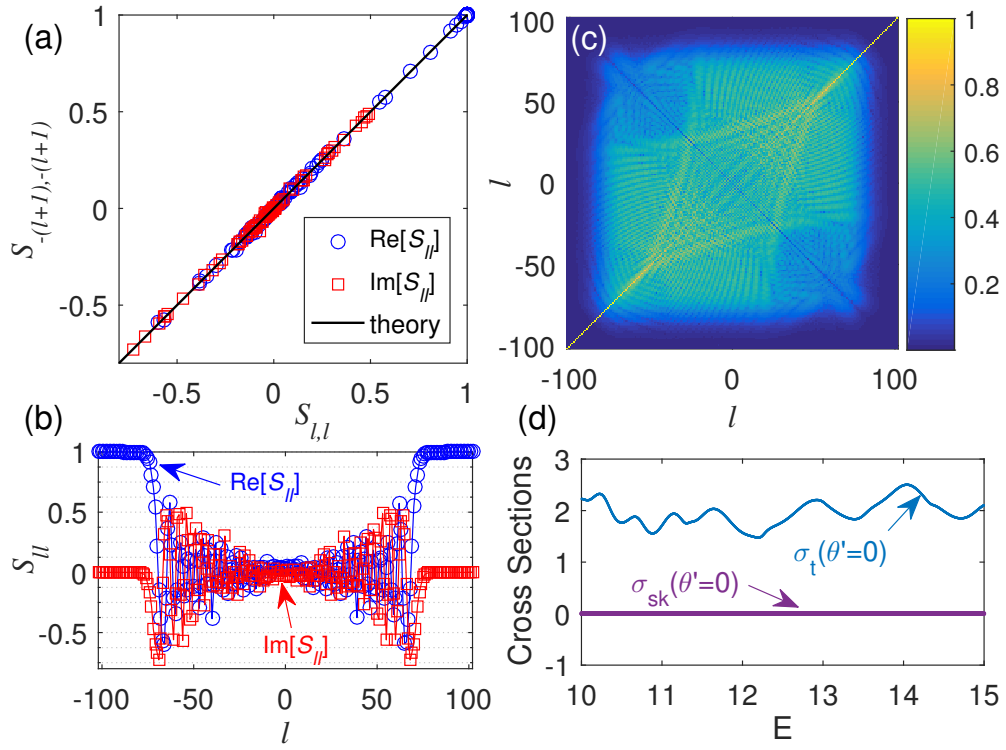

FIG. S1. **Validation of the S-matrix approach through the closed-form analytic constrains imposed by the symmetry of the system**. (a) Plot of the diagonal elements $S_{-(l+1),-(l+1)}$ versus S_{ll}, where the thick black line is the theoretical prediction of Eq. (S6.49), (b) real and imaginary parts of S_{ll}, (c) false color-coded map of the magnitudes of the full scattering matrix elements with a proper cut-off at $l = \pm 102$ (the scale bar shows the fourth root of magnitudes $|S_{ll'}|$); (d) the skew cross section σ_{sk} (purple line) and the total cross section σ_t (light blue curve) as a function of the energy for incident waves propagating parallel to the symmetry axis, where the vanishing skew (asymmetric) scattering, i.e., $\sigma_{sk} \equiv 0$, is consistent with the prediction of Eq. (S6.51). Parameters adopted for (a)-(c) are $E = 70$, $R_2/R_1 = 0.6$, $\xi = 0.3$, $v_1 = -140$, and $v_2 = 0$. For (d), the parameters are $R_2/R_1 = 0.6$, $\xi = 0.3$, $v_1 = -10$ and $v_2 = 40$.

VI. VALIDATION OF THE S-MATRIX APPROACH

A. Symmetry constraints

In spite of the lack of circular rotational symmetry, the system possesses a mirror (parity) symmetry, which imposes certain constrains on the S-matrix and leads to vanishing of skew (asymmetric) scattering provided that the incident wave propagates along the axis of the symmetry. In particular, for the configuration shown in Fig. 1(a) in the main text, for spinor scattering we can explicitly write the representation of the parity symmetry operation as $\mathcal{P}_x = \sigma_x \mathcal{R}_y$ with $\mathcal{R}_y$, which is the reflection operator that acts in the physical (position) space with respect to the x axis via the operations $x \to x(k_x \to k_x)$ and $y \to -y(k_y \to -k_y, \theta \to -\theta)$. As such, the system is invariant under parity, stipulating the relation $\mathcal{P}_x H \mathcal{P}_x^{-1} = H$ so that $\mathcal{P}_x \Psi$ is still a state of the system with the same energy. Under the operation of $\mathcal{P}_x$, the spinor cylindrical wave ${}^k h_m^{(1,2)}$ of given orbital angular

momentum m (corresponding to total angular momentum $L = m + 1/2$) can be transformed as

$$\begin{aligned}\mathcal{P}_x\, {}^k h_m^{(1,2)} &= i\sigma_x \mathcal{R}_y \begin{pmatrix} H_m^{(1,2)}(kr) \\ i\alpha H_{m+1}^{(1,2)}(kr) e^{i\theta} \end{pmatrix} e^{im\theta} = (-)^{m+1} i\alpha \begin{pmatrix} H_{-(m+1)}^{(1,2)}(kr) \\ i\alpha H_{-m}^{(1,2)}(kr) e^{i\theta} \end{pmatrix} e^{-i(m+1)\theta}, \\ &= (-)^{m+1} i\alpha\, {}^k h_{-(m+1)}^{(1,2)}.\end{aligned} \tag{S6.47}$$

Applying this relation to the resulting state $\Psi^{(0)}$ given in Eq. (S3.23), we obtain

$$\begin{aligned}\mathcal{P}_x \Psi^I &= \sum_m \mathcal{P}_x a_m^0 \mathcal{P}_x^{-1} \mathcal{P}_x \psi_m = \sum_{m=-\infty}^{\infty} \mathcal{P}_x a_m^0 \mathcal{P}_x^{-1} \mathcal{P}_x \left[{}^{k_0} h_m^{(2)} + \sum_{m'=-\infty}^{\infty} S_{mm'}\, {}^{k_0} h_{m'}^{(1)} \right], \\ &= \sum_{m=-\infty}^{\infty} \overline{a}_m^0 (-)^{m+1} i\alpha_0 \left[{}^{k_0} h_{-(m+1)}^{(2)} + \sum_{m'=-\infty}^{\infty} \mathcal{P}_x S_{mm'} \mathcal{P}_x^{-1} (-)^{m'-m}\, {}^{k_0} h_{-(m'+1)}^{(1)} \right], \\ &\equiv \sum_n c_n^0 \psi_n = \sum_{n=-\infty}^{\infty} c_n^0 \left[{}^{k_0} h_n^{(2)} + \sum_{n'=-\infty}^{\infty} S_{nn'}\, {}^{k_0} h_{n'}^{(1)} \right],\end{aligned} \tag{S6.48}$$

with deduced identities $n \equiv -(m+1)$, $n' \equiv -(m'+1)$, $c_n^0 \equiv \overline{a}_m^0 (-)^{m+1} i\alpha_0 = \mathcal{P}_x a_m^0 \mathcal{P}_x^{-1} (-)^{m+1} i\alpha_0$. We thus have

$$S_{nn'} \equiv S_{-(m+1),-(m'+1)} = \mathcal{P}_x S_{mm'} \mathcal{P}_x^{-1} (-)^{m'-m} = (-)^{m'-m} S_{mm'}. \tag{S6.49}$$

In particular, for $m = m'$, i.e., the diagonal elements, we have $S_{mm} = S_{-(m+1),-(m+1)}$. Under such constrains and using the definition of $f_l(\theta')$ given in Eq. (S2.17), we have

$$\begin{aligned}f_l(\theta') &= \sum_m a_m(\theta')(S_{ml} - \delta_{ml})(-i)^l, \\ &= \sum_m \frac{i^m e^{-im\theta'}}{2\sqrt{2}} \left[(-)^{m-l} S_{-(m+1),-(l+1)} - \delta_{-(m+1),-(l+1)} \right] (-i)^{2l+1} (-i)^{-(l+1)}, \\ &= e^{i\theta'} \sum_m \frac{i^{-(m+1)} e^{-i(m+1)\theta'}}{2\sqrt{2}} \left[S_{-(m+1),-(l+1)} - \delta_{-(m+1),-(l+1)} \right] (-i)^{-(l+1)}, \\ &= e^{i\theta'} \sum_{m'} a_{m'}(-\theta') \left[S_{m',-(l+1)} - \delta_{m',-(l+1)} \right] (-i)^{-(l+1)} \equiv e^{i\theta'} f_{-(l+1)}(-\theta').\end{aligned} \tag{S6.50}$$

For $\theta' = 0$ (π), i.e., when the incident wave propagates parallel (anti-parallel) to the axis of the mirror symmetry, we obtain $f_l = \pm f_{-(l+1)}$, based on which we can rewrite the skew cross section in Eq. (S2.18d) as

$$\begin{aligned}\sigma_{sk}|_{\theta'=0(\pi)} &= \frac{4}{k} \sum_l \Im[f_l f_{l+1}^*] = \frac{4}{k} \Im \left\{ |f_0|^2 + \sum_{l=0}^{\infty} \left[f_l f_{l+1}^* + f_{-(l+1+1)} f_{-(l+1)}^* \right] \right\}, \\ &= \frac{4}{k} \Im \left[|f_0|^2 + \sum_{l=0}^{\infty} 2\Re(f_l f_{l+1}^*) \right] \equiv 0.\end{aligned} \tag{S6.51}$$

These basic symmetry induced, exact constrains given by the closed forms in Eqs. (S6.49) and (S6.51) can serve as benchmarks for validating the S-matrix approach. Note that, while theoretically the dimension of the S-matrix is infinite, in practice a finite truncation is needed for a given

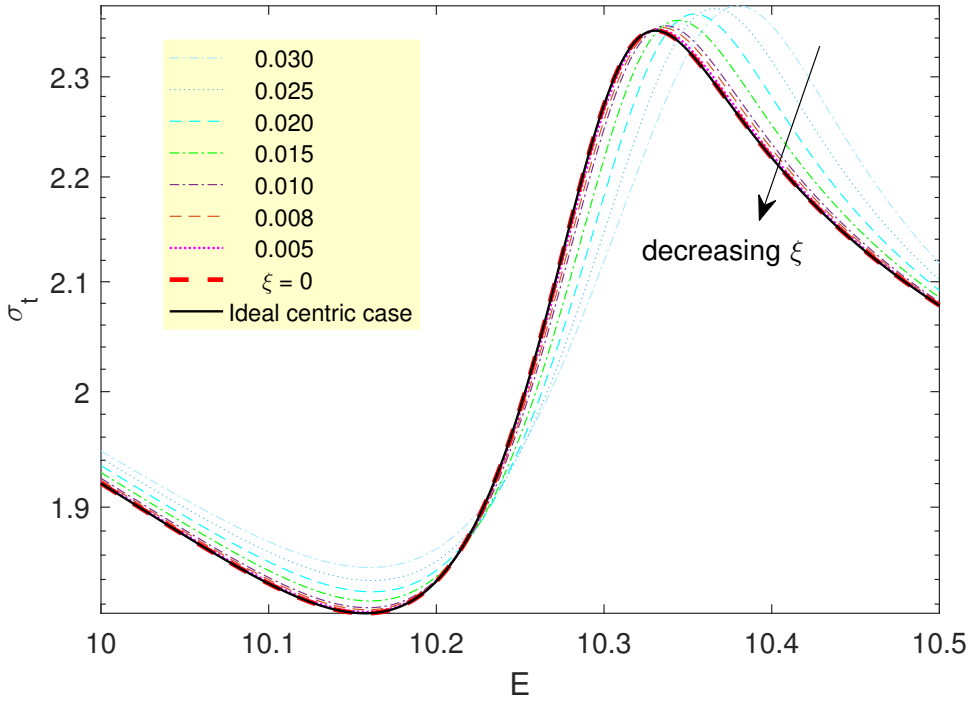

FIG. S2. **Validate the S matrix approach by showing the convergence to the integrable case**. For the case of classically integrable dynamics, the agreement between the theoretically predicted cross section values [the black curve calculated from Eqs. (S5.46b)] and the numerical results as ξ approaches zero. Parameters are $R_2/R_1 = 0.6$, $v_1 = -10$, and $v_2 = 40$.

energy E since channels with higher angular momenta $l \gg ER/\hbar v$ cannot be excited effectively and thus have negligible contribution to the scattering process. Representative results are shown in Fig. S1. We obtain a good agreement between the theoretical prediction and the simulation results from properly truncated S-matrices.

B. The case of $\xi \to 0$

Numerically, it is straightforward to validate the S-matrix approach indirectly by evaluating the convergence of the value of the cross section to the theoretical value for the limiting case of $\xi \to 0$ at which the classical dynamics are integrable. As shown in Fig. S2, a good agreement is achieved for $\xi < 0.01$.

VII. FULL DATA SET FOR THE PLOT FIG. 2(C) IN THE MAIN TEXT

Figure S3(a) shows the spin polarization versus ξ and the Fermi energy E, where the deep sky-blue regions in the energy domain indicating higher values of spin polarization become extended as ξ is increased and exceeds the value of 0.2. Figure S3(b) shows the average spin conductivities versus ξ, where the conductivity for the spin up population is a deceasing function of ξ but that for

the spin down state is essentially constant. Thus, on average the spin up particles undergo significantly stronger backward scattering as compared with the spin down particles, generating a severe spin imbalance (e.g., for $\xi = 0.3$) and consequently, significantly enhanced spin polarization. To appreciate the role of deformation played in generating a strong Dirac quantum chimera state, we calculate the average differential cross section $\Delta\overline{\sigma}_{diff} \equiv (E_2 - E_1)^{-1} \int_{E_1}^{E_2} (\sigma^{\uparrow}_{diff} - \sigma^{\downarrow}_{diff}) dE$ versus the backward scattering angle θ for two cases: $\xi = 0$ and $\xi = 0.3$, as shown in Fig. S3(c). A schematic illustration of the generation of spin polarization is shown in Fig. S3(d).

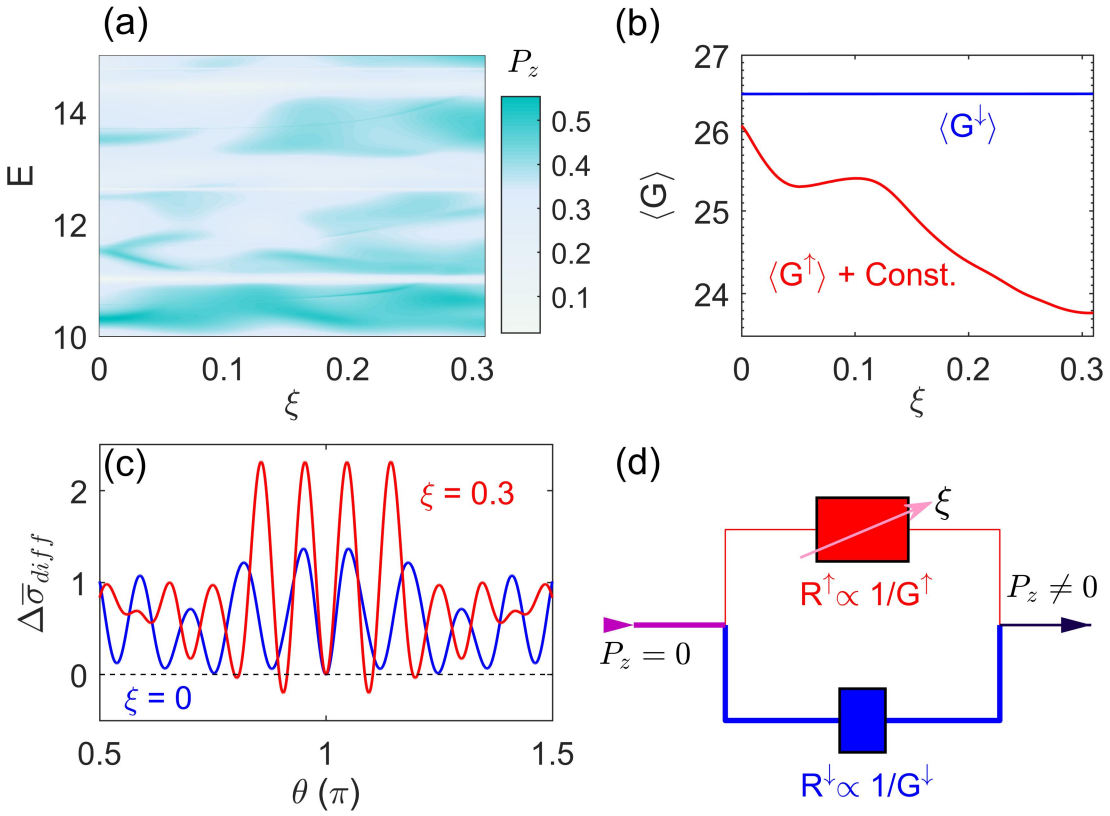

FIG. S3. **Spin polarization enhancement as a result of Dirac quantum chimera**. (a) Color-coded map of spin polarization P_z as a function of energy E and eccentricity ξ, (b) spin conductivities averaged over a given Fermi energy range versus ξ, where the red curve is vertically shifted by an arbitrary amount for better visualization, (c) illustration of a chaos rendered spin rheostat tuned by ξ, and (d) a schematic illustration of the generation of spin polarization.

VIII. FEASIBILITY OF EXPERIMENTAL IMPLEMENTATION

In general, the emergence of a Dirac chimera relies on the optical like behavior of Dirac electrons and Dirac cone splitting, which can be realized in current experimental systems of graphene. In particular, given the graphene lattice constant and typical values of the Fermi wavelength (e.g., $\lambda_F \sim 20$nm), a Dirac description of the step potential requires the length scale characterizing the junction sharpness to be $d \sim 1$nm, which has been recently achieved experimentally for a circular

junction geometry [5]. The size of the junction can be tuned to the micrometer scale ($\gg \lambda_F$), validating the short wavelength approximation [6]. Furthermore, the experimentally achievable strength of the exchange potential for graphene is strong enough to enable Dirac cone splitting at the room temperature [7], providing a base for experimentally observing the predicted Dirac quantum chimera.

---

[1] E. P. Wigner, Phys. Rev. **98**, 145 (1955).

[2] F. T. Smith, Phys. Rev. **118**, 349 (1960).

[3] H. Schomerus, M. Marciani, and C. W. J. Beenakker, Phys. Rev. Lett. **114**, 166803 (2015).

[4] D. Zwillinger, *Table of Integrals, Series, and Products* (Elsevier Science, 2014).

[5] C. Gutierrez, L. Brown, C.-J. Kim, J. Park, and A. N. Pasupathy, Nat. Phys. **12**, 1069 (2016).

[6] Y. Jiang, J. Mao, D. Moldovan, M. R. Masir, G. Li, K. Watanabe, T. Taniguchi, F. M. Peeters, and E. Y. Andrei, Nat. Nanotech. **12**, 1045 (2017).

[7] P. Wei, S.-W. Lee, F. Lemaitre, L. Pinel, D. Cutaia, W.-J. Cha, F. Katmis, Y. Zhu, D. Heiman, J. Hone, and J. S. M. C.-T. Chen, Nat. Mater. **15**, 711 (2016).